Paper No.
03341

CORROSION 2003

CORROSION IN MULTIPHASE FLOW CONTAINING SMALL AMOUNTS OF H_2S

Bruce Brown, Kun-Lin Lee, Srdjan Nesic
Institute for Corrosion and Multiphase Technology
Ohio University
Athens, Ohio 45701

ABSTRACT

Experiments in a large-scale flow loop provide an example of a somewhat increased corrosion rate under multiphase flow conditions caused by a low concentration of H_2S in a CO_2 saturated environment. Under operating conditions that prevent scale formation, the addition of 3ppm H_2S in the gas phase increased the corrosion rate of AISI C 1018 and API 5L X-65 carbon steels, while the addition of H_2S concentrations of 15ppm and greater tended to retard corrosion. The same effect was not found in single-phase flow. A vapor-liquid equilibrium model for dilute aqueous solutions of H_2S/CO_2 was developed to provide a tool for estimating water chemistry of a closed system such as a flow loop or an autoclave.

Keywords: hydrogen sulfide, carbon dioxide, acid gas, vapor-liquid equilibrium model

INTRODUCTION

The simultaneous presence of CO_2 and H_2S in produced fluids makes for a very aggressive environment, which can lead to severe corrosion of mild steel. H_2S and CO_2 have been shown to produce competing films at temperatures between 20 and 60ºC[1]. When hydrogen sulfide is present in low concentrations in a CO_2 dominated system, some have noted that the iron sulfide (FeS) film interferes with the formation of the iron carbonate scale ($FeCO_3$). However, the iron sulfide film is considered to have a protective effect at about 60°C[1]. Although a protective film forms in the presence of H_2S, observations by Videm and Kvarekval[2] demonstrated that small amounts of H_2S increased the corrosion rate because the film could easily be disturbed by surface defects and the attack did not produce uniform corrosion. This is of interest because the iron sulfide film is more easily removed from the pipe wall than the iron carbonate scale. Under turbulent conditions (i.e. slug flow), removal of the "protective" scale can occur and lead to an increased corrosion rate and possibly pitting corrosion.

There are a limited number of studies that cover H_2S corrosion, particularly when compared to the extensive literature available on "sweet" CO_2 corrosion. The few experimental studies that have been published in open literature[2,3,4,5] are limited to autoclaves and glass cells. Previous research has shown that low concentrations of H_2S (<30 ppm) in a CO_2 saturated water solution can accelerate the corrosion rate. The effect seems to vanish at higher H_2S concentrations and high temperatures[3,5] (>80°C) when a protective film forms. In one study it was also suggested that the effect of H_2S could be significant only in the low pH range[4] (<pH 5); an important factor not considered in any of the other studies. In general, the reasons behind the "H_2S effect" on CO_2 corrosion are not entirely understood. It has been speculated that adsorbed sulfide species and/or sulfide films accelerate the corrosion rate of mild steel through a catalytic or a galvanic effect.[4]

This present research program was directed to investigate the effect of small amounts of H_2S on CO_2 corrosion of mild steel in single- and two-phase flow in a multiphase flow loop. In order to minimize the precipitation of films, this study was conducted at pH 4. The principal questions addressed are:

1. Can the phenomenon of the CO_2 corrosion rate acceleration at low H_2S concentration, the "H_2S effect," be reproduced in a strictly controlled single- and two-phase flow loop experiment?
2. Does this "H_2S effect" disappear at higher H_2S concentrations?
3. Is the "H_2S effect" dependent upon flow velocity?
4. Is the "H_2S effect" dependent on the flow regime (single-phase vs. stratified vs. slug flow)?

EXPERIMENTAL PROCEDURE

System details

The experimental set-up and operation of the multiphase flow loop has previously been described[10] and is shown in Figure 1. A modification has been made since the initial documentation, a new test section was put in place to allow WL (weight loss), ER (electrical resistance), and LPR (linear polarization resistance) monitoring in single phase flow as well as in multiphase flow; the location is shown in Figure 2. These three additional probe locations allow for seven (7) simultaneous corrosion rate measurement devices to be used in the three separate test sections.

Corrosion measurement

After the solution was deoxygenated and saturated with the CO_2 gas, H_2S was added. Subsequently, the corrosion probes were inserted under pressure. WL, ER, and LPR flush mount probe elements were inserted in specific locations and the order remained constant throughout the testing procedure. Elements tested in single-phase flow (in order of the direction of flow) were WL, ER, and LPR. Elements tested in the upstream multiphase flow section were WL and LPR. Elements tested in the downstream multiphase flow were WL and ER. The order of probe insertion for each test was single-phase, multiphase upstream, and then into multiphase downstream test sections.

Weight loss coupons are 0.45" (1.14cm) diameter, 0.125" (0.318cm) thick, carbon steel, with a slight bevel on the reverse edge for press-fit, were flush mounted in a nylon holder. Four coupons will fit in the nylon holder that is attached to a holding rod with a flat head stainless steel screw. Each coupon is

labeled with a number and orientation mark prior to being polished to a 600-grit finish, weighed to the nearest ten-thousandth (0.0001) gram, and mounted in the holder according to coupon number and orientation. Each coupon is mounted in the holder so that the orientation mark will show the coupons' orientation to flow after the experiment is completed.

Electrical resistance probes are 10μm working thickness, flush-mount, modular style probes with the corroding material for these probes made of AISI C 1010 carbon steel. The probes used for linear polarization are designed in a "concentric ring" style. In between each electrode surface is a non-conductive epoxy.

As coupons and probes were removed from the system after each test, the surface of each was lightly rinsed with isopropyl alcohol to remove water. WL coupons to be used for weight loss were cleaned by hand. Each coupon was rubbed with a clean cotton cloth using isopropyl alcohol as a cleaning agent. The coupon was allowed to dry, weighed, and stored in a desiccator. WL coupons to be used for scanning electron microscopy (SEM) analysis remained in dry storage until removal for examination; WL coupons for cross section analysis were mounted in clear epoxy, cut, polished, and gold sputter-coated prior to SEM.

$CO_2/H_2S/H_2O$ vapor-liquid equilibrium model

It was found by repetitive measurements (using gas chromatography) that in a closed loop system, the small amount of H_2S is consumed through adsorption and corrosion; therefore, there is a need for continual replenishment to maintain a specific concentration of H_2S. In order to facilitate this procedure, development of a simple vapor-liquid equilibrium model was initiated. This model had to be flexible enough to help us identify the existing concentration of H_2S in the water phase based upon gas phase measurement and to predict the amount of added H_2S necessary to return to the desired conditions.

The $CO_2/H_2S/H_2O$ vapor-liquid equilibrium model for dilute aqueous solutions was programmed to simulate two different environments: an "open" system with a constant excess of gas mixture partial pressure of CO_2 and H_2S, and a "closed" system similar to an autoclave or a flow loop system that can have varying gas/liquid volume ratios. The model is based on the vapor-liquid equilibria of gaseous species and the dissociation equilibria for dissolved species.

Open system conditions. In an open system, due to an unlimited supply of gas, there is a constant partial pressure of carbon dioxide and hydrogen sulfide gaseous species on the surface of the water. Vapor-liquid equilibrium of carbon dioxide and hydrogen sulfide reactions are described as:

$$CO_{2(g)} \Leftrightarrow CO_{2(aq)} \quad (1)$$

$$H_2S_{(g)} \Leftrightarrow H_2S_{(aq)} \quad (2)$$

Once carbon dioxide dissolves in water, $CO_{2(aq)}$ is involved in a sequence of chemical reactions as follows:

Hydration of aqueous carbon dioxide:

$$CO_{2(aq)} + H_2O_{(aq)} \xleftrightarrow{Khyd} H_2CO_{3(aq)} \quad (3)$$

Dissociation of carbonic acid:

$$H_2CO_{3(aq)} \xleftrightarrow{Kca} H^+_{(aq)} + HCO^-_{3(aq)} \quad (4)$$

Dissociation of bicarbonate ion:

$$HCO^-_{3(aq)} \xleftrightarrow{Kbi} H^+_{(aq)} + CO^{2-}_{3(aq)} \quad (5)$$

When hydrogen sulfide dissolves in water, we have:

Dissociation of Hydrogen sulfide:

$$H_2S \xleftrightarrow{K1} H^+_{(aq)} + HS^-_{(aq)} \quad (6)$$

Dissociation of HS^- ion:

$$HS^-_{(aq)} \xleftrightarrow{K2} H^+_{(aq)} + S^{2-}_{(aq)} \quad (7)$$

Since all these processes occur in water, dissociation of water is also included in the model:

$$H_2O_{(aq)} \xleftrightarrow{Kw} H^+_{(aq)} + OH^-_{(aq)} \quad (8)$$

With the partial pressures of both gaseous species known in an open system, Henry's law can be applied in order to calculate the vapor-liquid equilibria of (1) and (2):

$$[CO_2]\, H_{CO_2} = P_{CO_2} \quad (9)$$

$$[H_2S]\, H_{H_2S} = P_{H_2S} \quad (10)$$

Where $[CO_2]$ and $[H_2S]$ are the concentrations of carbon dioxide and hydrogen sulfide in solution, respectively, and H is the Henry's constant. P_{CO_2} and P_{H_2S} are the partial pressure of carbon dioxide and hydrogen sulfide, respectively.

Once the concentration of dissolved carbon dioxide and dissolved hydrogen sulfide are fixed, the reactions (3)-(8) shown above can be described by equilibria reactions as follows:

$$K_{hyd} = \frac{[H_2CO_3]}{[CO_2][H_2O]} \quad (11)$$

$$K_{ca} = \frac{[H^+][HCO_3^-]}{[H_2CO_3]} \quad (12)$$

$$K_{bi} = \frac{[H^+][CO_3^{2-}]}{[HCO_3^-]} \quad (13)$$

$$K_1 = \frac{[H^+][HS^-]}{[H_2S]} \quad (14)$$

$$K_2 = \frac{[H^+][S^{2-}]}{[HS^-]} \quad (15)$$

$$K_W = \frac{[H^+][OH^-]}{[H_2O]} \quad (16)$$

The equilibrium constants, K, are a function of the temperature and are available in the open literature[6]. Since the solution cannot have a net charge, an electroneutrality relation is required. Mathematically, this is expressed as:

$$[H^+] + [Na^+] = [HS^-] + 2\times[S^{2-}] + [HCO_3^-] + 2\times[CO_3^{2-}] + [Cl^-] \quad (17)$$

Additional species such as Fe^{2+}, Na^+, and Cl^- need to be considered in this equation when present.

Closed system conditions. In a closed system, such as an autoclave or a flow loop, the partial pressure of gases is not constant and the concentration of H_2S and CO_2 in gaseous phase becomes an unknown when the vapor-liquid equilibrium is disturbed (i.e. by a change of pH). However, the total amount of carbonic and sulfide species are constant in a closed system. Hence, two extra mass conservation equations for both species are added in order to describe the closed system.

$$\Sigma[carbonic\ species] = [CO_{2(g)}] + [CO_{2(aq)}] + [H_2CO_{3(aq)}] + [HCO_{3(aq)}^-] + [CO_{3(aq)}^{2-}] = \text{constant} \quad (18)$$

$$\Sigma[sulfide\ species] = [H_2S_{(g)}] + [H_2S_{(aq)}] + [HS_{(aq)}^-] + [S_{(aq)}^{2-}] = \text{constant} \quad (19)$$

With these two equations, the system of equations is closed and can be solved to obtain species concentrations.

Numerical method of solution. There are eleven species that existed in our flow loop system: $CO_{2(g)}$, $CO_{2(aq)}$, H_2CO_3, HCO_3^-, $CO_3^{=}$, $H_2S_{(g)}$, $H_2S_{(aq)}$, HS^-, $S^{=}$, H^+, OH^-. Therefore there are eleven unknowns to be solved in eleven equations in a closed system: two vapor-liquid equilibria (9,10), six chemical

equilibria (11,12,13,14,15,16), an electroneutrality equation (17) and two mass balance equations (18,19). Newton-Raphson's method was chosen for solving this system of non-linear algebraic equations. A FORTRAN program for the calculation of the equilibrium compositions was written with the following sequence of calculations:

1. The temperature, total pressure, desired H_2S concentration in gas phase, initial concentration of the salt and the volume of the gaseous and aqueous phase in the system are specified.
2. The partial pressure of water vapor, H_2S and CO_2 are calculated.
3. The preliminary estimate is refined using Newton-Raphson's method for the iterative solution of non-linear equations.
4. The equilibrium composition is determined from the converged solution.

If the pH is adjusted by setting the H^+ concentration to desired value, this apparently leads to an over specified problem (ten unknowns with eleven equations). However, an additional unknown is introduced here (e.g. the concentration of Na^+) in order to change the pH.

Validation of the equilibrium model

Simulation of a hypothetical closed system showing the effect of pH on the carbonic species concentration is shown in Figure 3. Note that this is a simulation for a pure CO_2 condition. More HCO_3^- and CO_3^{2-} are produced by dissociation as the pH increases, while the concentration of $CO_{2(aq)}$ and H_2CO_3 decreases. At high pH (pH>10), the concentration of HCO_3^- starts decreasing. Eventually most of the carbonic species would be converted into CO_3^{2-}.

The next test for the model was to simulate the equilibrium chemistry in our H_2S flow loop system. The following parameters were used: 60°C, pH 4, $p(CO_2)$= 7.7 bar, 3 ppm H_2S in the gas phase, and a system gas-to-liquid ratio of 1004:946. By using the model, the amount of H_2S that was required to achieve certain gaseous concentrations can be pre-determined under these experimental conditions. The calculated values were verified within 10% of the experimental measurements when using a gas chromatograph to measure the gas phase concentration.

Figure 4 demonstrates the comparison between equilibrium conditions in the H_2S flow loop system and a hypothetical open system such as a gas pipeline over the wide range of pH in the presence of 3 ppm of H_2S in gas phase. By comparing the sulfide species only, the concentrations in the two systems are the same over the pH range of 4-6. The concentrations only deviate at pH>6. Because the hypothetical open system simulates the field condition with a limitless gas supply, this proves that the H_2S flow loop system is capable of simulating successfully the water chemistry of a field condition in the pH range between 4-6.

In order to illustrate the amount of sulfide species in relation to the carbonic species, Figure 5 shows all the species concentrations. Note that the y-axis is log scale and the concentration of carbonic species is greater than the sulfide species by several orders of magnitude. The concentration of carbonic species is not altered by the presence of 3 ppm of H_2S in the system.

H_2S/CO_2 experiments

Test parameters are listed in Table 1 both for single-phase flow and two-phase flow experiments; these parameters were chosen from the indicative studies of previous research[2,3,4,5]. Both single-phase flow and multiphase-flow experiments were run simultaneously in different sections of the test loop. A set of twenty (20) experiments were conducted (4 H_2S/CO_2 ratios × 5 velocities). A comparison of H_2S ppm concentration by mass in the gas phase used throughout this paper to CO_2/H_2S ratio is shown in Table 2. To relate these ratios to others from literature, a graphic from Pots[11], redrawn to scale in Figure 6 with 100ppm and 500ppm H_2S concentration lines added, shows the ratios used in this experiment are considered to be in the "sweet CO_2 corrosion regime". Previous studies[2,3,4,5] used for comparison range from 3 to 450ppm by volume H_2S with CO_2/H_2S ratios from 310,000 to 2,200 respectively, which also places them in the "sweet CO_2 corrosion regime" that is defined as a CO_2/H_2S ratio greater than 500[11].

Each series of tests (based upon H_2S/CO_2 ratio) consisted of one 24-hr experiment and four 4-hr experiments that covered a range of superficial liquid velocities from 0.2 to 2.0 m/s. The 24-hr experiment with Vsl = 1.0 m/s utilized WL coupons, LPR, and ER to measure the corrosion rate, while the four-hour tests at superficial liquid velocities of 0.2, 0.5, 1.5, and 2.0 m/s were limited to LPR and ER due to their quicker response time. To compare the corrosion rates calculated from 4-hr experiments and 24-hr experiments, data from the 24-hr experiments were analyzed and categorized to provide the calculated values shown in Table 3. As expected in most cases, the corrosion rate during the first 4 hours of the test is somewhat higher than the stabilized corrosion rate 20 hours later. To compare ER and LPR corrosion rate values directly with WL corrosion rate values, the 24-hr integrated corrosion rate values were used; to compare ER and LPR across different liquid velocities, the 4-hr integrated corrosion rate data were used. Although corrosion rate does decrease almost 30% in each case from the 4-hr integrated value to the 24-hr final stabilized corrosion rate, the trends established in each data set are similar.

Figure 7 and Figure 8 show the change in corrosion rate for different H_2S/CO_2 ratios as a function of time for each of the 24-hr experiments at Vsl = 1.0 m/s as measured by LPR. Note the high corrosion rate measured during exposure to 3 ppm H_2S in multiphase flow. When corrosion rates measured in multiphase flow are grouped together, as in Figure 9, the 3ppm concentration appears to show the highest corrosion rate for H_2S in the system. This is considered to be the "H_2S effect" of high CO_2/H_2S ratio environments. This effect is not seen in single-phase flow for any of the three corrosion rate measurement techniques used. Figure 10, Figure 11, Figure 12, and Figure 13 compare corrosion rate measurements for each of the specific methods in multiphase and single-phase flow. Both the LPR and WL coupons are in agreement with the H_2S effect seen, but the ER probe gives consistent readings for the 0 and 3 ppm concentrations.

A third set of data also agrees with the previous findings in the comparison of materials in a slightly sour environment. Figure 14 and Figure 15 show the comparison of WL corrosion rate measurements for coupons made of AISI C 1018 and API 5L X-65 exposed to H_2S/CO_2 ratios from 0 to 100 ppm in single phase and multiphase flow, respectively. Both materials are in agreement with the "H_2S effect" seen in multiphase flow and not seen in single-phase flow. It should be noted that in all cases when concentration of H_2S was larger than 15 ppm, a significant retardation of the corrosion rate was obtained.

Figure 16, Figure 17, Figure 18, and Figure 19 show the relationships of corrosion rate to a change in flow velocity. Each of these figures uses the integrated corrosion rate over the first 4 hours of each

experiment for the following comparisons. Both ER and LPR methods show an increase in corrosion rate from single-phase flow to multiphase flow at the same liquid velocity, but provide different conclusions in respect to the effect of a change in flow velocity on the corrosion rate. The ER probe information shown in Figure 16 and Figure 17 shows an increase in corrosion rate with an increase in flow velocity for both single phase and multiphase flow. The LPR corrosion rate data shown in Figure 18 and Figure 19 does not show an effect of flow velocity on corrosion rate.

Lengthing the test time

The first set of experiments show the corrosion rate peak in less than 5 hours of initial exposure and a stabilization of the corrosion rate occurring in less than 24 hours as shown by LPR data in Figure 7 and Figure 8. Testing was also conducted to compare the corrosion rates developed over longer periods of time. Under conditions of 0.79MPa CO_2, 100ppm H_2S and 60ºC, liquid and gas superficial gas velocities have been maintained as Vsl = 1.0 m/s for both single phase and multiphase, and Vsg = 3.0 m/s for multiphase. After 24 hours exposure to system conditions, the slope of the change in corrosion rate per hour (Δ(mm/yr)/hour) as measured by LPR is less than 10%. After 45 hours, this same slope is less than 1% in each case and diminishes over time. Figure 20 shows the comparison of this change in corrosion rate with time using LPR data for six data sets: three experimental conditions displaying single phase (SP) and multiphase (MP) results. Similar results were obtained by ER measurements and show proof that the system has developed a constant corrosion rate after less than 24 hours of exposure.

Surface analysis

Due to the fragile nature of the films produced at 60ºC, film thickness measurement has been a more difficult comparison to achieve. Scanning electron microscopy (SEM) and electron dispersion spectroscopy (EDS) analysis were used for evaluating the films produced. An SEM of a surface defect on AISI C 1018 coupon after 24-hour exposure to multiphase flow in closed system conditions with 100ppm H_2S in the gas phase is shown in Figure 21. When the area inside the surface defect was analyzed with EDS, no sulfur peak was detected, but EDS analysis of the surface area shown as Figure 21 produced the spectrum shown in Figure 22 proving that sulfide film growth has occurred. The cross sectional view of this film from a similar 24-hour exposure time and conditions show a film of sub-micron proportions is visible as a thin white line, shown in Figure 23, but is not substantial enough for characterization.

By lengthening the exposure time to 72 hours, a more substantial product layer has been produced as shown in Figure 24. Because this measurable 10µm corrosion product layer was also seen in exposure times of 96 and 120 hours under the same conditions, another series of experiments are planned for a comparison at the 96-hour exposure time. The corrosion product layers shown in Figure 25 and Figure 26 are from single phase and multiphase flow exposures, respectively, for AISI C 1018 steel exposed to 0.79MPa CO_2, 100ppm H_2S, 60ºC for 96 hours.

CONCLUSION

- The phenomenon of the CO_2 corrosion rate acceleration at a low H_2S concentration was observed under conditions of 60°C and 0.79MPa CO_2 at 3ppm H_2S only in multiphase flow. The phenomenon of the "H_2S effect" has been reproduced in a multiphase flow system at low concentrations of H_2S in a CO_2 saturated environment. This "effect" diminishes at concentrations in excess of 15ppm in the gas phase and does not appear to be dependent upon flow velocity or flow regime.
- Corrosion rate measurements by linear polarization and weight loss of AISI C 1018 and API 5L X-65 steels show this phenomenon of increased corrosion rate in multiphase flow, but not in single-phase flow.
- As the concentration of H_2S was increased above 10 ppm, the corrosion rate significantly decreased. At 60°C and 0.79MPa CO_2, iron sulfide film growth on coupons exposed to 100 ppm H_2S in the gas phase will decrease the corrosion rate within 24 hours of exposure in both single-phase and multiphase flow conditions.
- In association with the retardation of the corrosion rate by exposure to 100ppm H_2S, analysis of the surface by SEM and EDS provide proof of a thin surface film resistant to flow that grows with time in both single phase and multiphase conditions.

REFERENCES

1. Srinivasan, S., and Kane, R.D., "Prediction of Corrosion Rates of Steel in CO_2/H_2S Production Environments," Prevention of Pipeline Corrosion Conference, Houston, TX, 1995.

2. Videm, K., and Kvarekval, J., "Corrosion of Carbon Steel in CO_2 Saturated Aqueous Solutions Containing Small Amounts of H_2S," NACE CORROSION/94, Paper No. 12, 1994.

3. Ikeda, A., Ueda, M., and Mukai, S., "Influence of Environmental Factors on Corrosion in CO_2 Source Well," Advances in CO_2 Corrosion, Vol. 2, 1985.

4. Kvarekval, J., "The Influence of Small Amounts of H_2S on CO_2 Corrosion of Iron and Carbon Steel," EUROCORR '97, Trondheim, Norway.

5. Valdes, A., Case, R, Ramirez, M., and Ruiz, A., "The Effect of Small Amounts of H_2S on CO_2 Corrosion of a Carbon Steel," Paper No. 22, CORROSION/98.

6. B. E. Roberts and P.R. Tremaine, "Vapour Liquid Equilibrium Calculations for Dilute Aqueous Solutions of CO_2, H_2S, NH_3 and NaOH to 300^{o}C", The Canadian Journal of Chemical Engineering, 63, (1985): p.294-300.

7. R.D. Deshmukh and A.E. Mather, "A Mathematical Model for Equilibrium Solubility of Hydrogen Sulfide and Carbon Dioxide in Aqueous Alkanolamine Solutions", Chemical Engineering Science, 36, (1980): p.355-362.

8. A. Miyasaka, "Thermodynamic Estimation of pH of Sour and Sweet Environments as Influenced by the Effects of Anions and Cations", CORROSION/92, paper no. 247.

9. A. Anderko and R.Young, "Simulation of CO_2/H_2S corrosion using thermodynamic and electrochemical models", CORROSION/99, paper No.31

10. Brown, B., Schubert, A., "The Design and Development of a Large-Scale, Multiphase Flow Loop for the Study of Corrosion in Sour Gas Environments," Paper 02502, CORROSION/2002.

11. Pots, B. F. M., John, R.C., et al, "Improvements on de-Waard Milliams Corrosion Prediction and Applications to Corrosion Management," Paper #02235, CORROSION/2002.

TABLES

Table 1. Experimental Parameters

PARAMETERS	CONDITIONS
Temperature	60°C
Partial Pressure CO_2 (P_{CO_2})	7.9×10^5 Pa
Fluid	100% synthetic seawater, pH 4
H_2S / CO_2 ratios (mass)	0, 3, 15, & 100 ppm
V_{sl} (single-phase and two-phase flow)	0.25, 0.5, 1.0, 1.5, & 2.0 m/s
V_{sg} (two-phase flow)	3 m/s
Dissolved oxygen	< 20 ppb
Dissolved iron	< 10 ppm

Table 2. Comparison of H_2S/CO_2 mass ratio to H_2S mol% and CO_2/H_2S ratio.

Temperature / C	H_2S ppm (by mass)	H_2S partial pressure (Pa)	H_2S ppm by volume (mol%)	pCO_2 / pH_2S
60	3	3.10	3.8	2.5E+05
60	15	15.49	19.1	5.1E+04
60	100	103.28	127.5	7.6E+03
80	3	3.14	3.8	2.5E+05
80	15	15.71	18.8	5.0E+04
80	100	104.73	125.1	7.5E+03

Table 3. Empirical Corrosion Rate Calculation Method Comparison

H_2S / CO_2 Ratio	Single Phase / Multiphase	4 hr integrated value	24 hr integrated value	24 hr final corrosion rate	4 hr integrated value	24 hr integrated value	24 hr final corrosion rate
ppm H_2S	SP / MP	ER (mm/yr)	ER (mm/yr)	ER (mm/yr)	LPR (mm/yr)	LPR (mm/yr)	LPR (mm/yr)
0	SP	15.9	13.3	12.5	12.8	7.3	7.9
3	SP	3.4	3.9	3.9	5.9	5.8	3.3
15	SP	7.0	6.6	6.7	1.2	1.0	0.9
100	SP	2.0	1.7	1.6	3.3	2.0	1.2
0	MP	17.4	12.8	13.7	7.3	6.1	6.6
3	MP	11.3	12.0	11.8	19.7	15.1	10.8
15	MP	2.8	1.7	1.4	3.7	3.6	3.6
100	MP	2.4	4.9	5.4	3.6	2.7	1.9

FIGURES

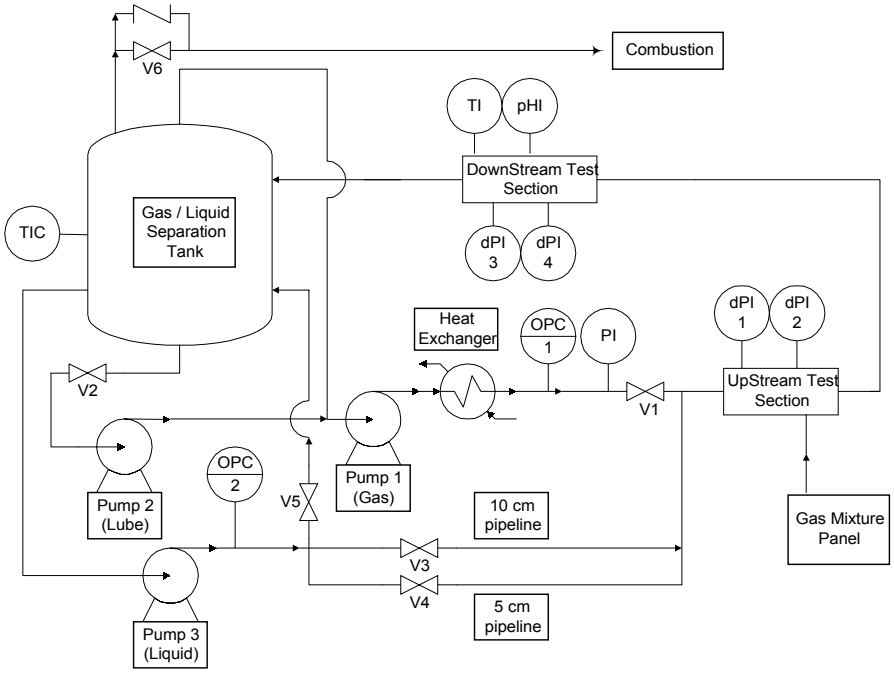

Figure 1. Original Schematic diagram of Multiphase flow loop (P&ID).

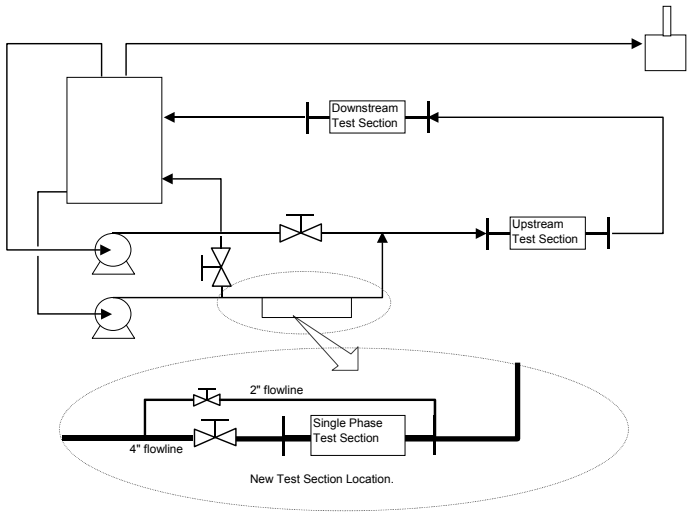

Figure 2. Location of new pipe section for single phase flow testing.

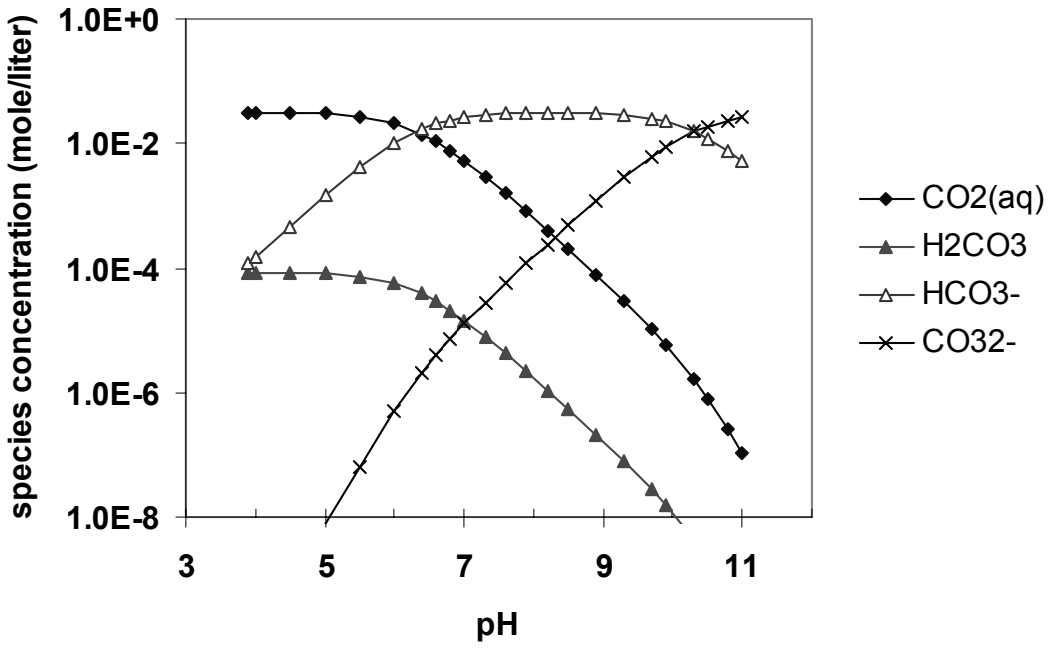

Figure 3. pH effect on the concentration of carbonic species for 25°C, atmospheric pressure in closed system

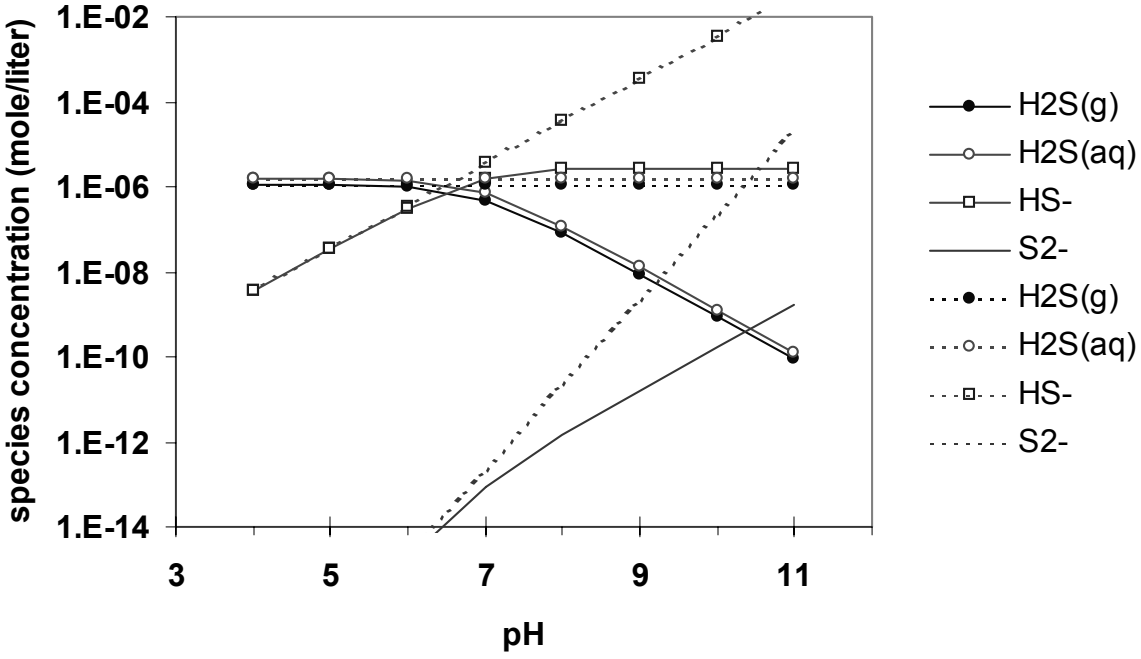

Figure 4. Effect of pH on the concentration of sulfide species, solid line=H_2S closed flow loop system with gas to liquid volume ratio of 1004:946, dash line = open system.

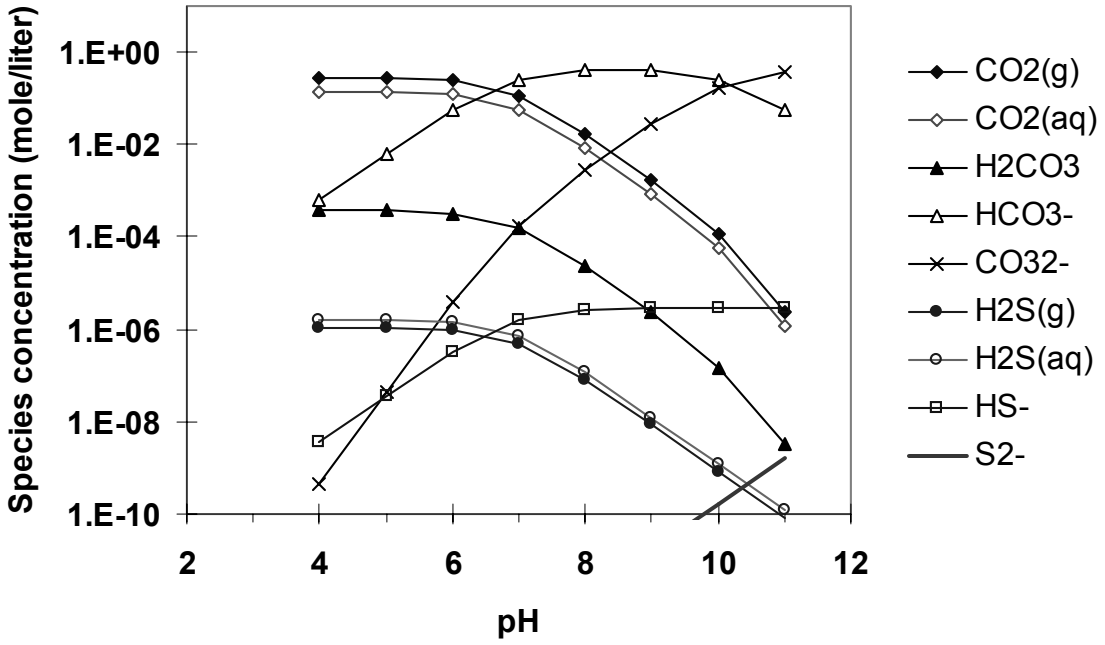

Figure 5. H_2S flow loop system concentration of all the species in the presence of 3 ppm H_2S at T=60°C, pCO_2= 7.9 bar with gas to liquid ratio of 1004:946

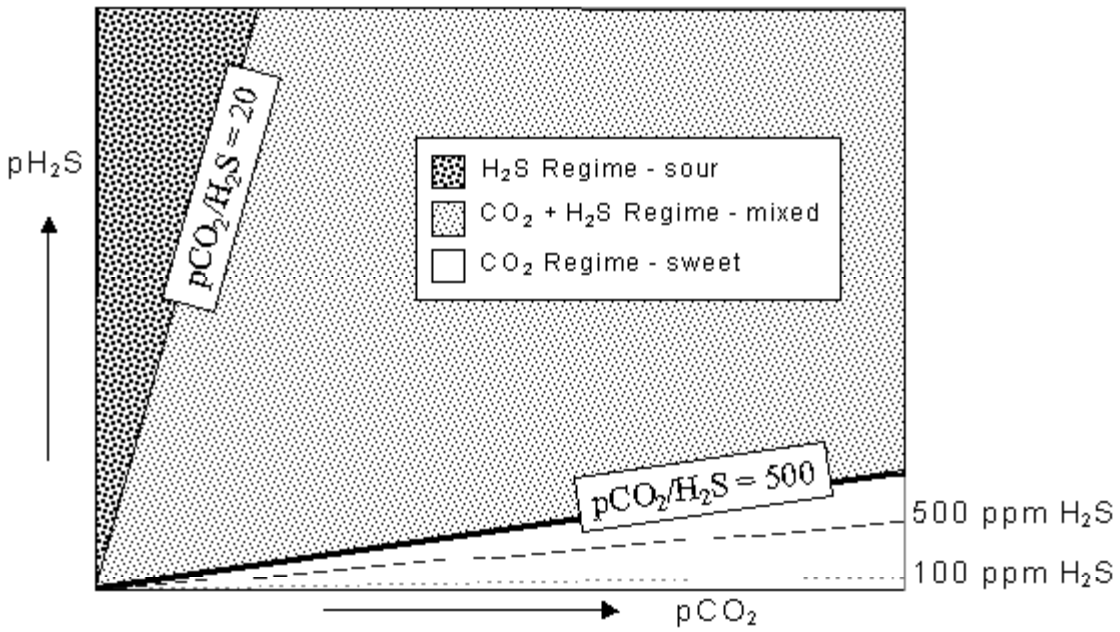

Figure 6. Corrosion regimes in CO_2/H_2S corrosion as defined by Pots, et al. and the present experiments (dashed lines)

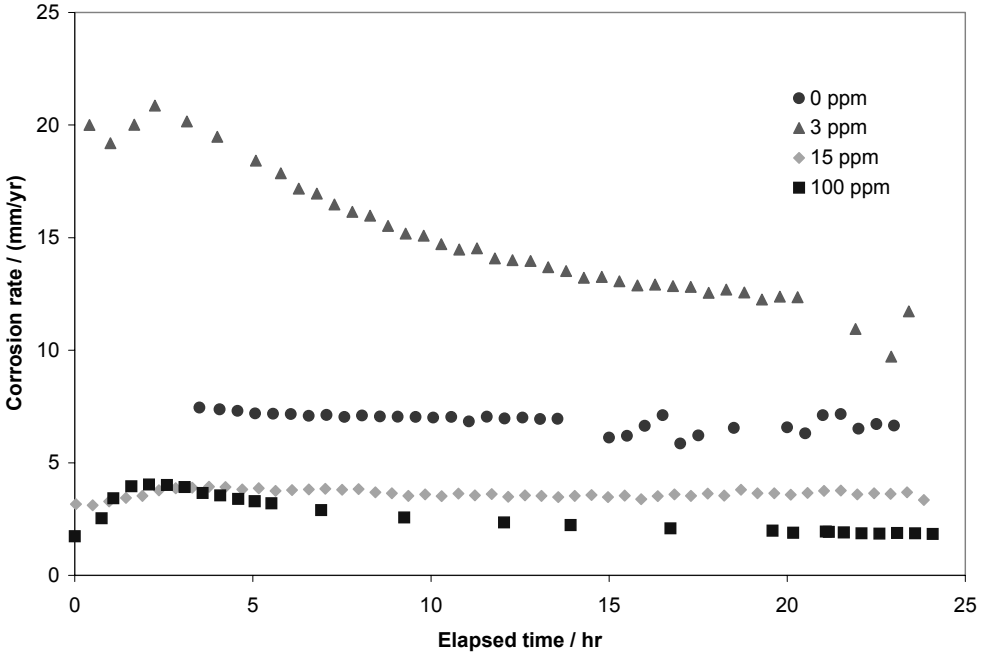

Figure 7. Corrosion rate vs. time by continuous LPR in multiphase flow for various concentrations of H_2S. (pCO_2 = 0.79MPa, pH=4.0, T=60ºC.)

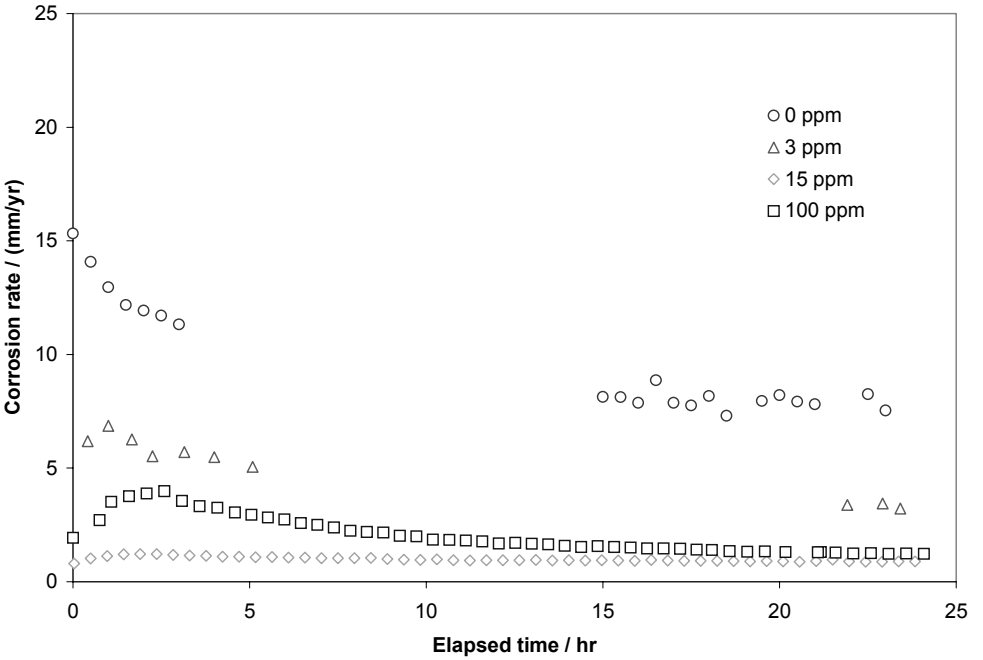

Figure 8. Corrosion rate vs. time by continuous LPR in single-phase flow for various concentrations of H_2S. (pCO_2 = 0.79MPa, pH=4.0, T=60ºC.)

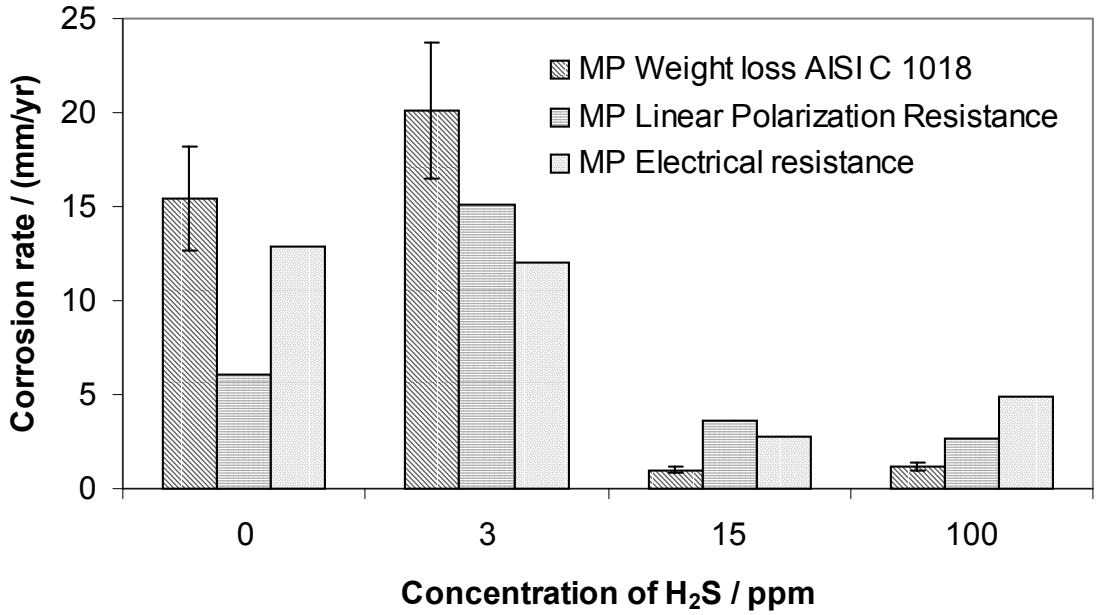

Figure 9. Corrosion rate vs. H_2S concentration for LPR, WL, and ER. (pCO_2 = 0.79MPa, pH = 4.0, Vsg = 3.0 m/s, and Vsl = 1.0 m/s.)

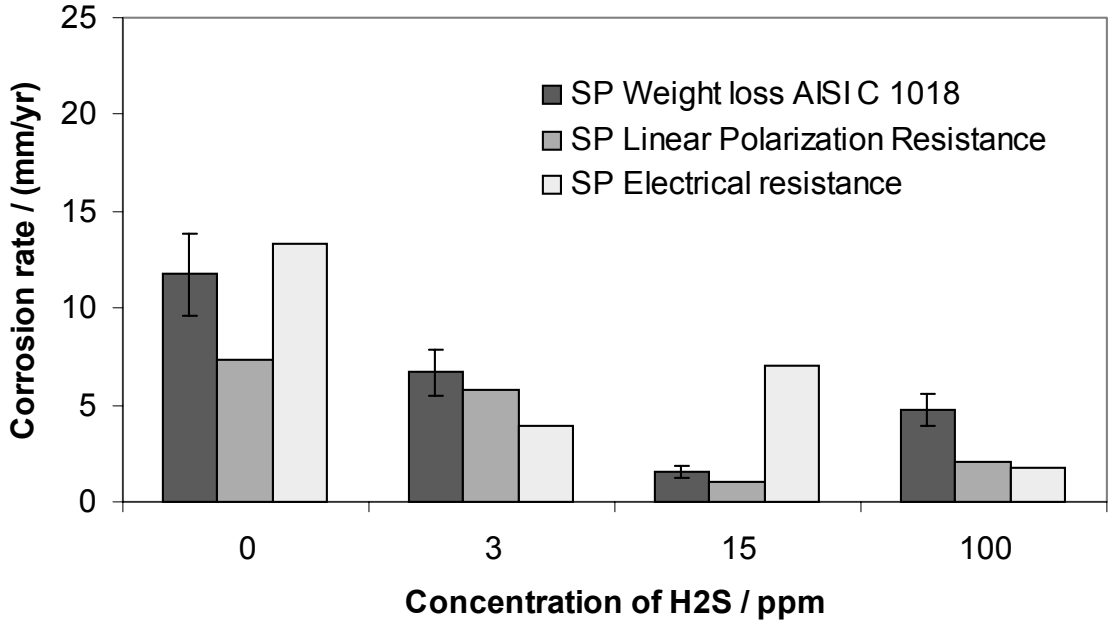

Figure 10. Corrosion rate vs. H_2S concentration for LPR, WL, and ER. (pCO_2 = 0.79MPa, pH = 4.0, and Vsl = 1.0 m/s.)

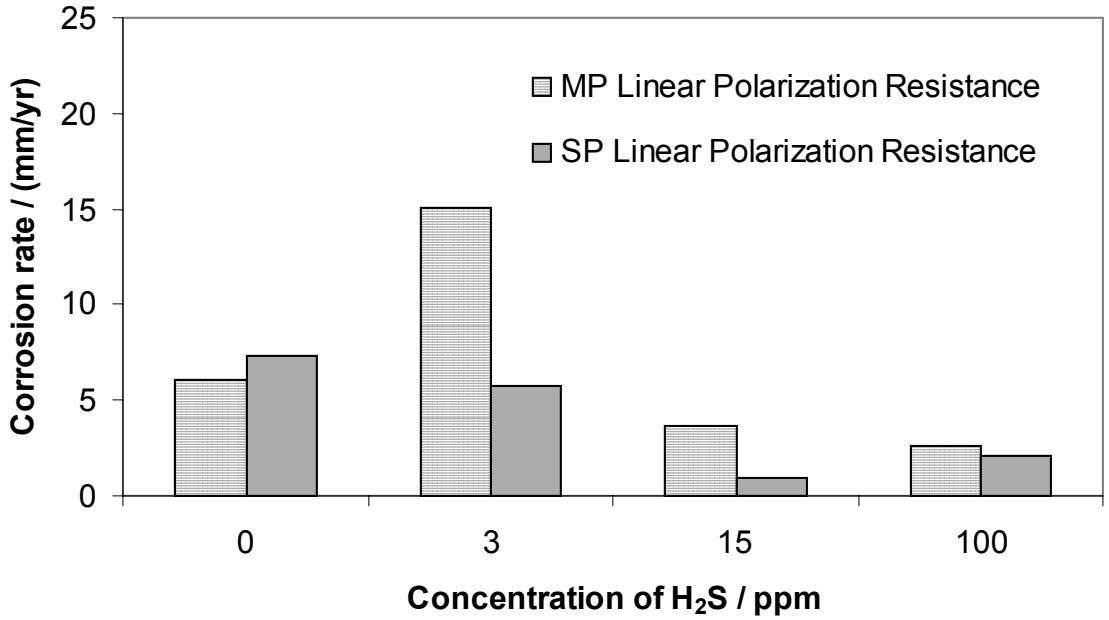

Figure 11. Corrosion rate vs. H_2S concentration for LPR in multiphase and single-phase flow. (pCO_2 = 0.79MPa, pH = 4.0, Vsg = 3.0 m/s, and Vsl = 1.0 m/s.)

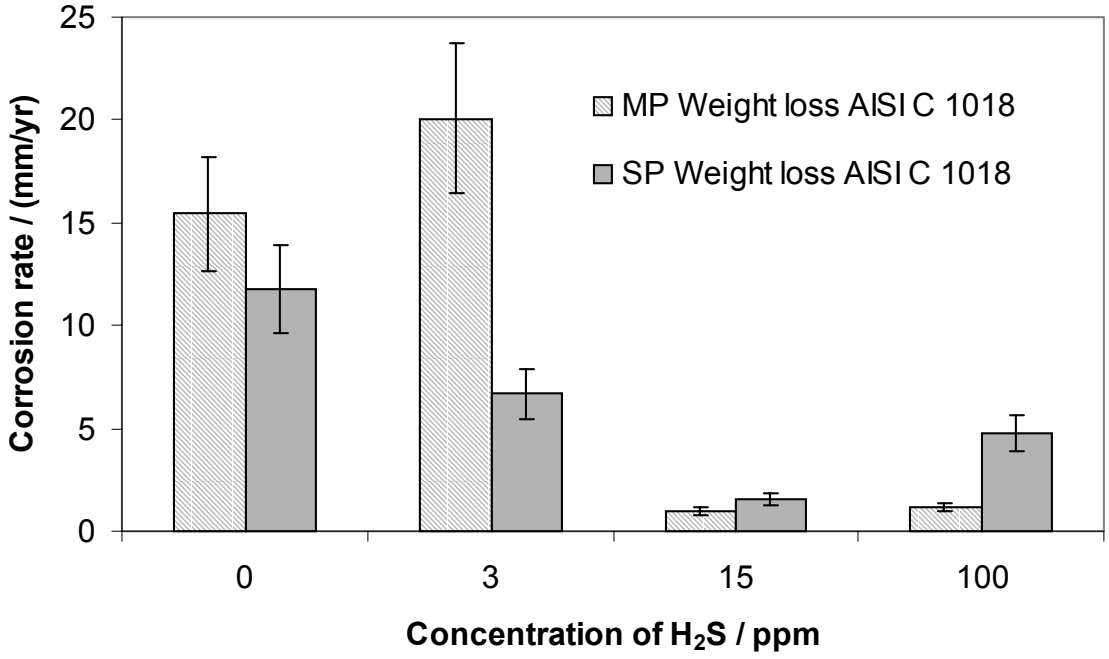

Figure 12. Corrosion rate vs. H_2S concentration for WL in multiphase and single-phase flow. (pCO_2 = 0.79MPa, pH = 4.0, and Vsg = 3.0 m/s, Vsl = 1.0 m/s.)

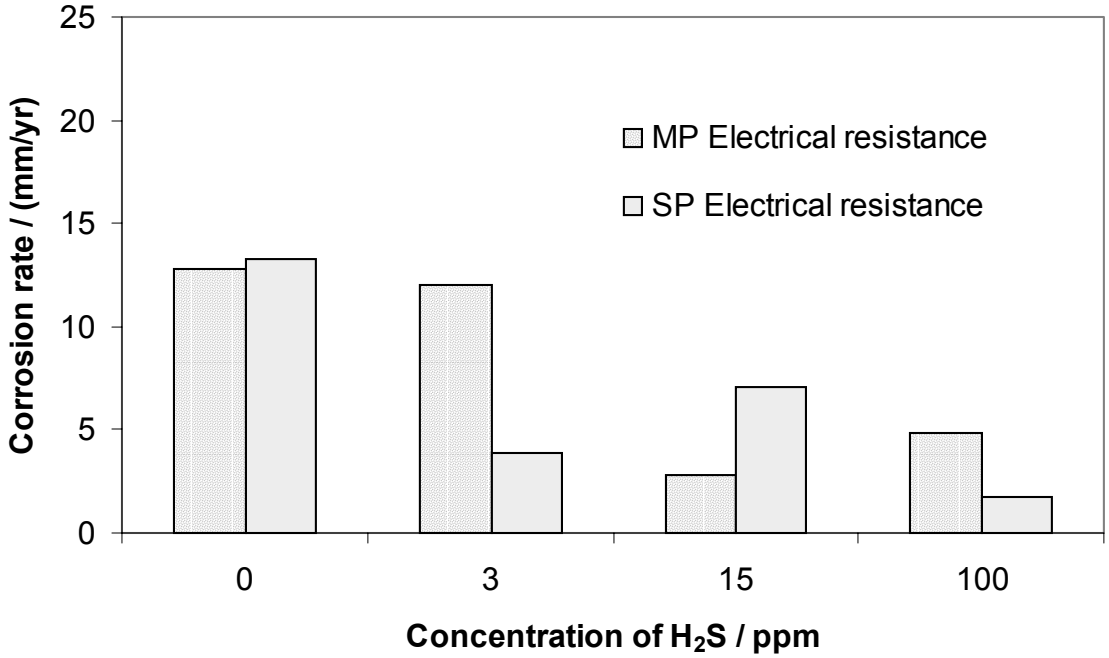

Figure 13. Corrosion rate vs. H_2S concentration for ER in multiphase and single-phase flow. (pCO_2 = 0.79MPa, pH = 4.0, and Vsg = 3.0 m/s, Vsl = 1.0 m/s.)

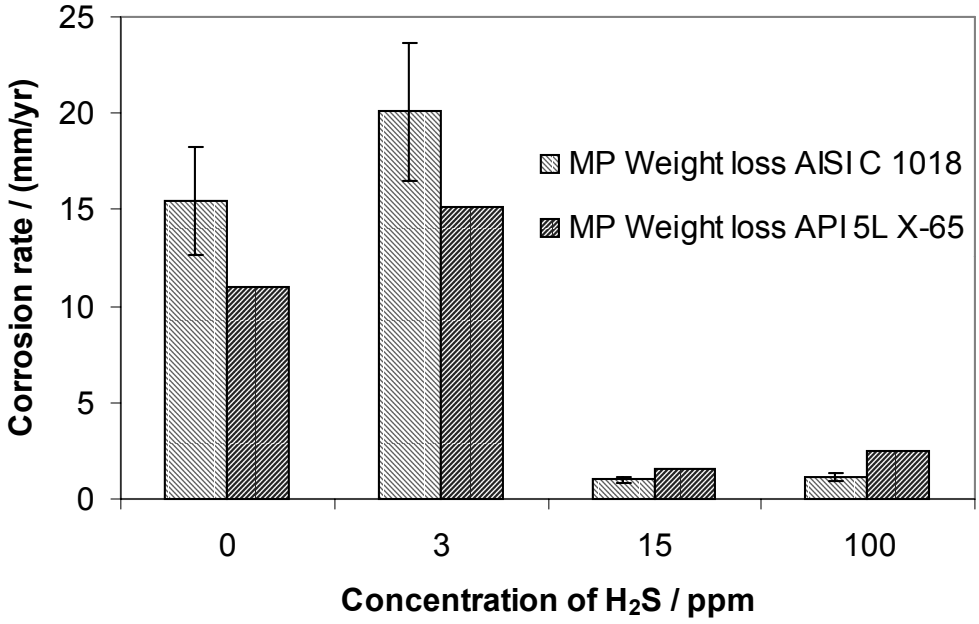

Figure 14. Corrosion rate vs. H_2S concentration for AISI C 1018 and API 5L X-65 materials in multiphase flow. (pCO_2 = 0.79MPa, pH = 4.0, Vsg = 3.0 m/s, and Vsl = 1.0 m/s.)

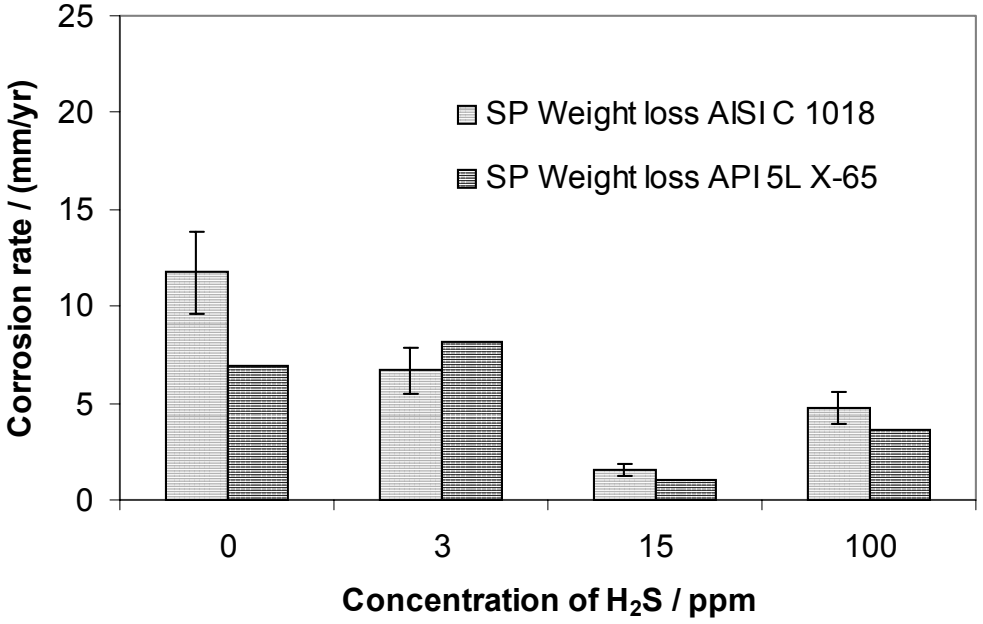

Figure 15. Corrosion rate vs. H_2S concentration for AISI C 1018 and API 5L X-65 materials in single-phase flow. (pCO_2 = 0.79MPa, pH = 4.0, and Vsl = 1.0 m/s.)

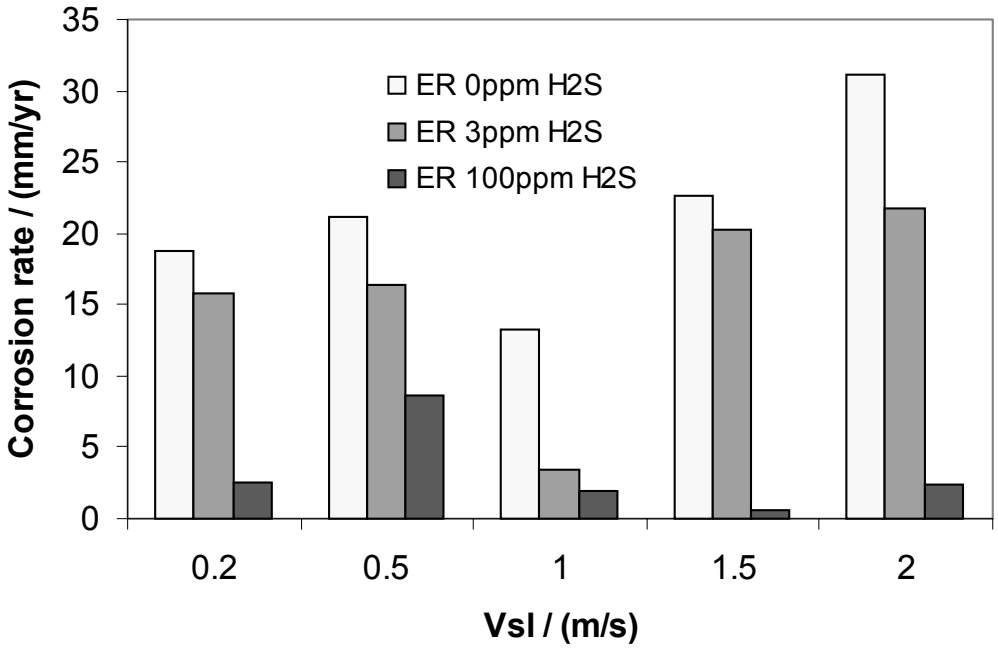

Figure 16. Corrosion rate vs. velocity for ER in single-phase flow. (pCO_2 = 0.79MPa, 60C.)

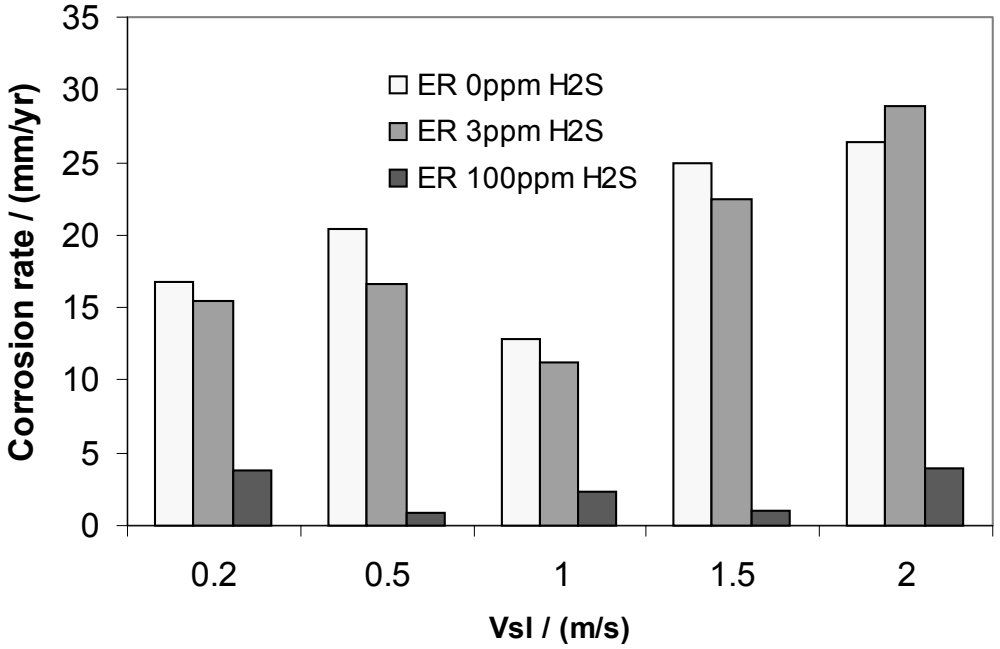

Figure 17. Corrosion rate vs. velocity for ER in multiphase flow. (Vsg = 3.0 m/s, pCO_2 = 0.79MPa, 60ºC.)

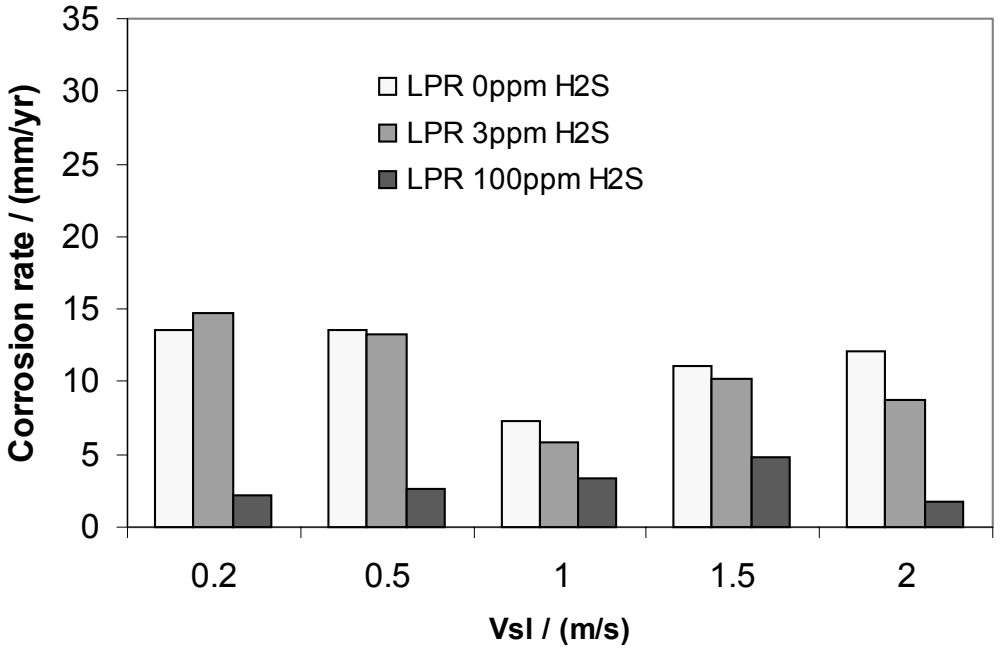

Figure 18. Corrosion rate vs. velocity for LPR in single phase flow. (pCO_2 = 0.79MPa, 60ºC.)

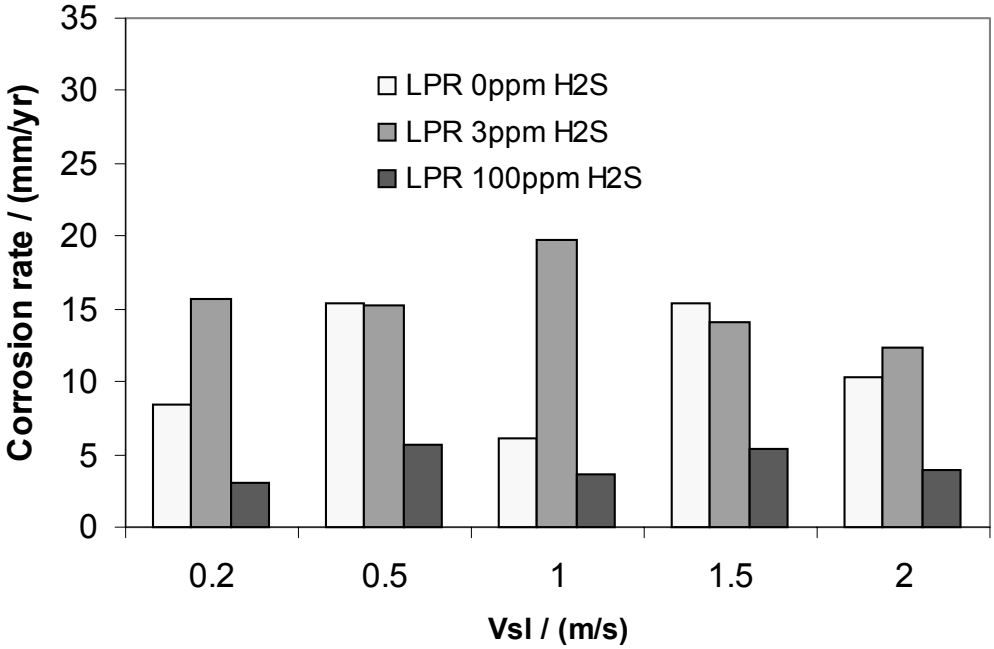

Figure 19. Corrosion rate vs. velocity for LPR in multiphase flow. (Vsg = 3.0 m/s, pCO_2 = 0.79MPa, 60ºC.)

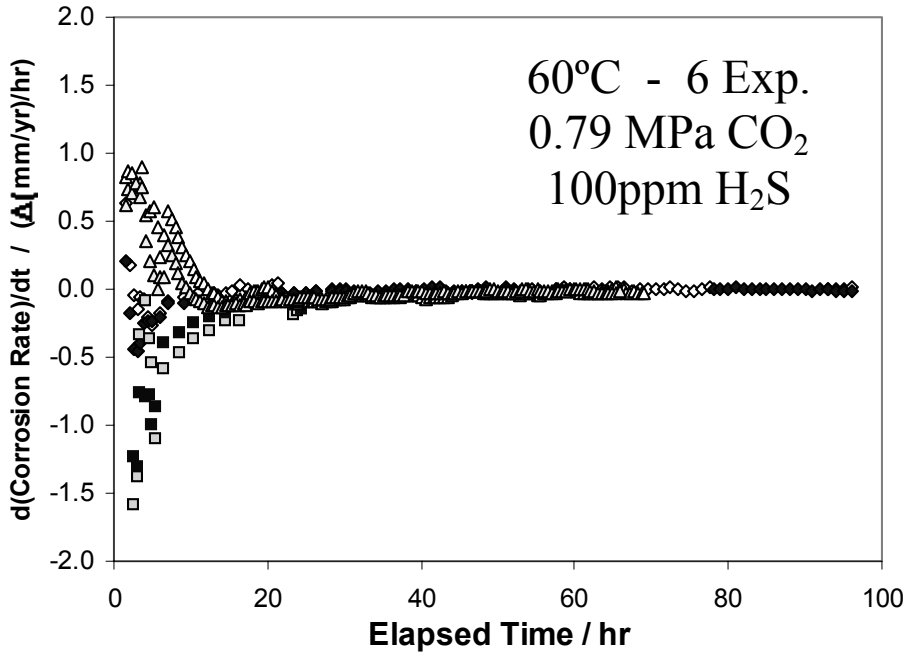

Figure 20. Comparison of the changes in corrosion rate with time over the length of each experiment for three different tests at 60ºC, 0.79MPa CO_2, 100ppm H_2S.

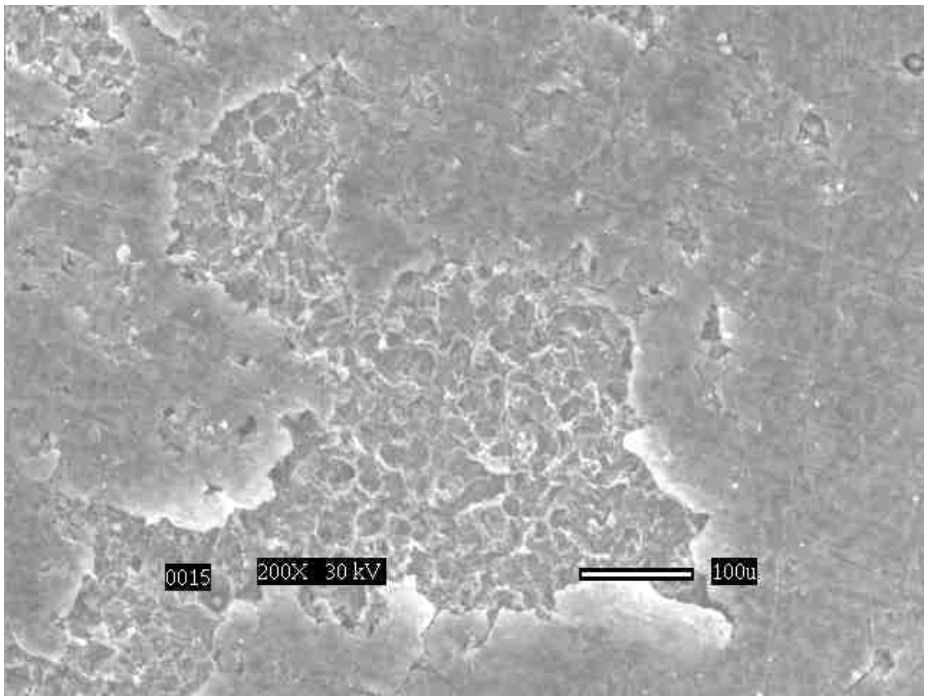

Figure 21. SEM of damaged film after coupon removal from 24 hour experiment, multiphase flow. (Vsg = 3.0 m/s, Vsl = 1.0 m/s, pCO_2 = 0.79MPa, 60ºC, 100% ASTM seawater, 100ppm H_2S.)

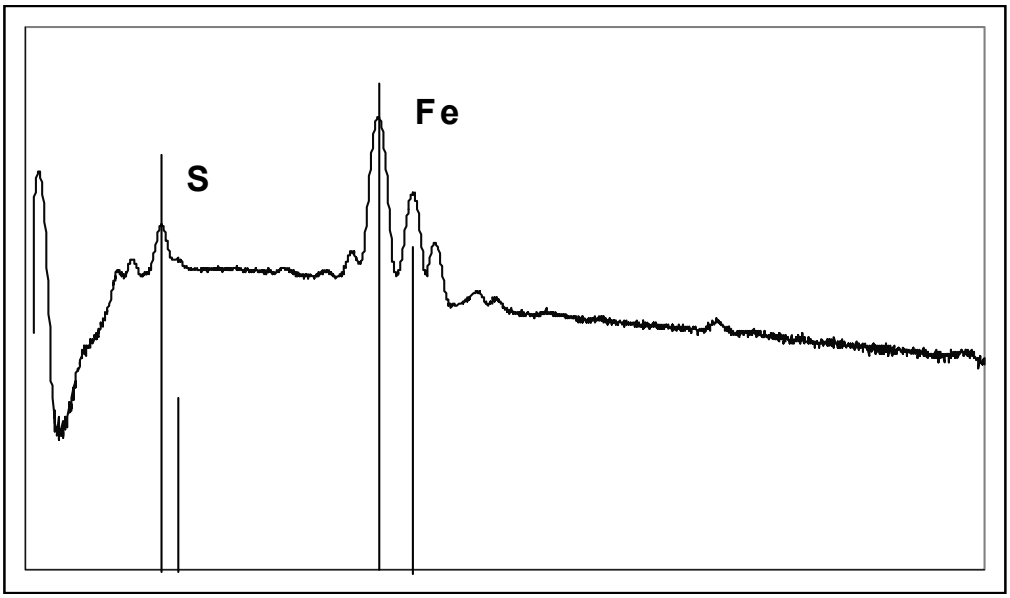

Figure 22. EDS of visual area shown in SEM photo Figure 21.

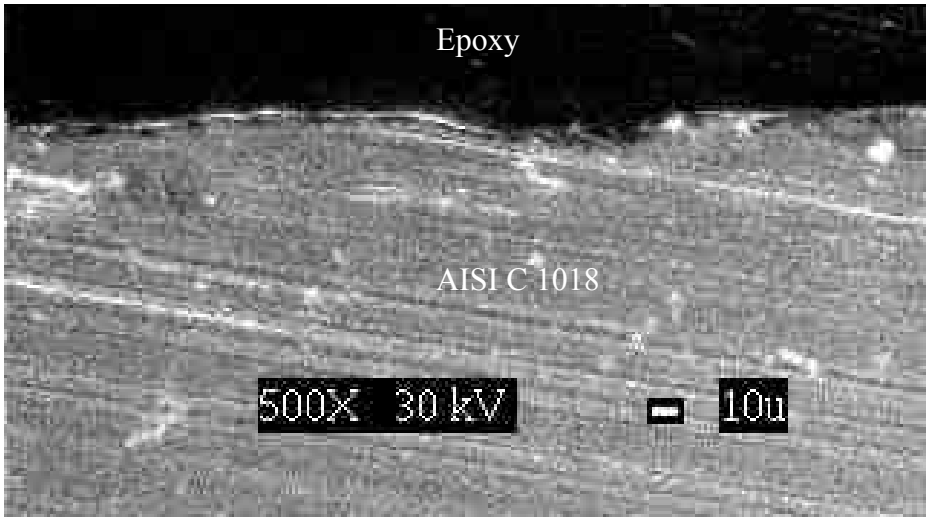

Figure 23. Corrosion product film on AISI C 1018 steel coupon. (24hrs, 0.79MPa CO_2, 100ppm H_2S, Vsg = 3 m/s, Vsl = 1 m/s, 60ºC)

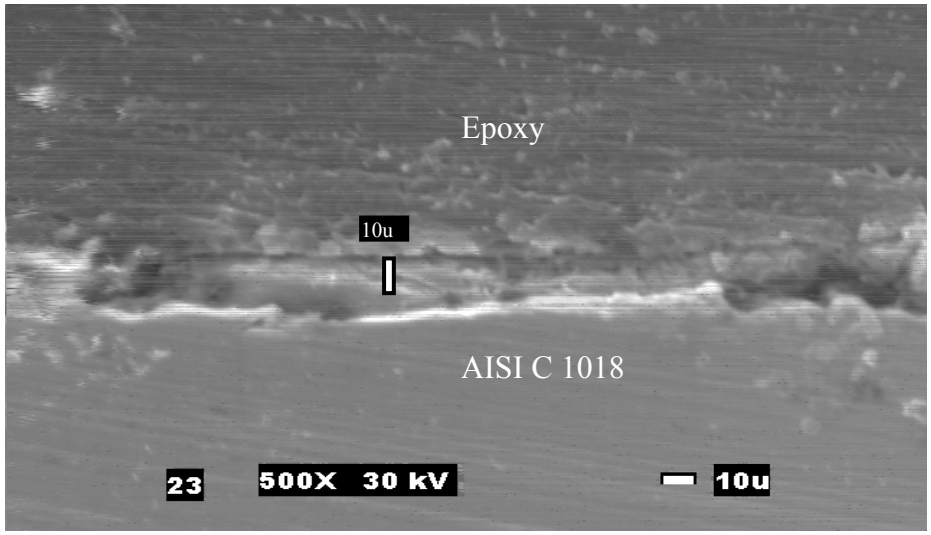

Figure 24. Corrosion product film on AISI C 1018 steel coupon exposed to multiphase conditions. (72hrs, 0.79MPa CO_2, 100ppm H_2S, Vsg = 3 m/s, Vsl = 1 m/s, 60ºC)

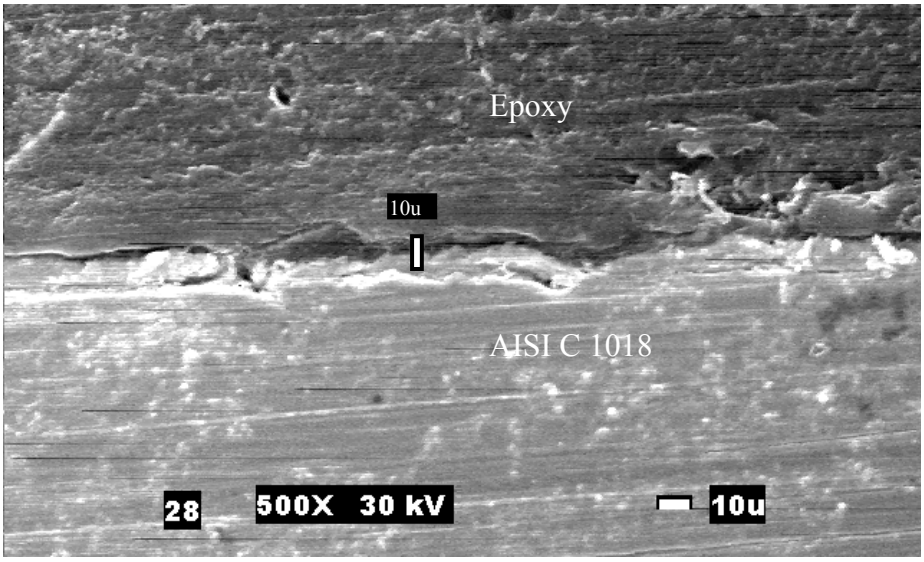

Figure 25. Corrosion product film on AISI C 1018 steel coupon exposed to single phase conditions. (96hrs, 0.79MPa CO_2, 100ppm H_2S, Vsl = 1 m/s, 60ºC)

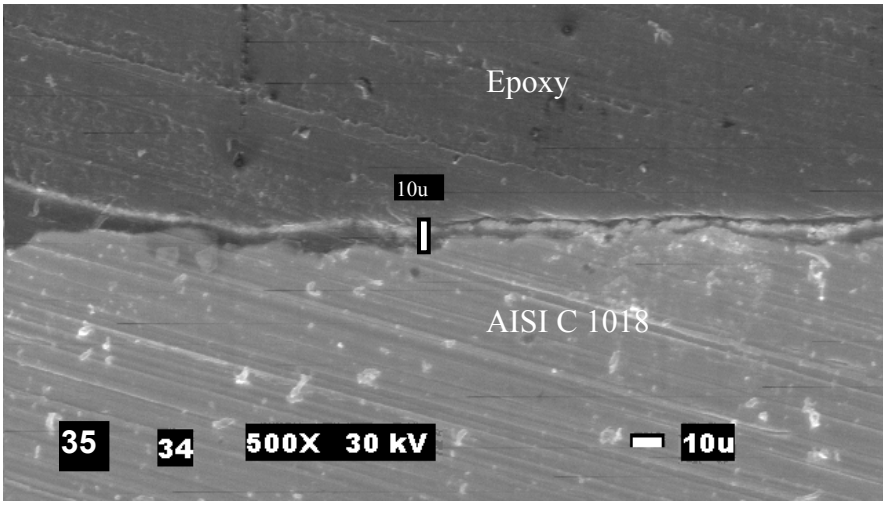

Figure 26. Corrosion product film on AISI C 1018 steel coupon exposed to multiphase conditions. (96hrs, 0.79MPa CO_2, 100ppm H_2S, Vsg = 3 m/s, Vsl = 1 m/s, 60ºC)